

# Dynamics of Saturated Energy Condensation in Two-Dimensional Turbulence

Chi-kwan Chan,<sup>1,\*</sup> Dhrubaditya Mitra,<sup>1,†</sup> and Axel Brandenburg<sup>1,2,‡</sup>

<sup>1</sup>*NORDITA, Roslagstullsbacken 23, 106 91 Stockholm, Sweden*

<sup>2</sup>*Department of Astronomy, Stockholm University, 106 91 Stockholm, Sweden*

(Dated: March 18, 2019)

We derive and numerically confirm that the saturation of energy condensation in two-dimensional turbulence is governed by the balance between forcing and small-scale dissipation. The time scale of saturation is inversely proportional to the viscosity but the saturation energy level is determined by both viscosity and the forcing scale. It is shown that, because the energy dissipation is proportional to the enstrophy, which itself is a conserved quantity in the ideal case, it is necessary to resolve the enstrophy spectrum to achieve numerical consistency. We also find that the movement of the condensate vortices can be described as Brownian motion of an inertial particle.

PACS numbers: 47.27.-i, 47.27.De, 47.27.E-

## I. INTRODUCTION

Two-dimensional (2D) hydrodynamic turbulence is very different from the three-dimensional one. In 2D, small vortices can merge to form bigger vortices. In other words, there is the possibility of an inverse cascade of energy. This is because the equations of ideal hydrodynamics in two dimensions have, in addition to energy, also enstrophy as a conserved quantity. With the addition of viscous dissipation and an external force at an intermediate scale, energy (inverse) cascades to larger length scales and enstrophy (direct) cascades to smaller length scales [1–3].

Let us now consider turbulence in a finite domain of size  $L$ . The smallest Fourier mode allowed in this system is  $k_1 = 2\pi/L$ . Due to the inverse cascade, energy piles up at  $k_1$ . This phenomenon, often called Bose condensation in 2D turbulence (see fig. 1) was first pointed out and studied by Smith and Yakhot [4, 5], and recently verified by numerical simulations [6] and laboratory experiments [7]. For a fixed non-zero viscosity,  $\nu$ , the energy of the condensate cannot grow without limit but saturates [8]. The saturation occurs at time scales of the order of  $1/\nu k_1^2$ . This is an unusual example in fluid turbulence where viscous effects play an important role in large length scales.

In this paper we show, by direct numerical simulations (DNS), that the saturation value of the energy of the condensate is not only determined by viscosity but also by the forcing wavenumber  $k_i$ . We also find that the direct enstrophy cascade must be well-resolved for accurate numerical determination of the saturation. Motivated by the analogy between the formation of large-scale structures in two-dimensional turbulence and the large-scale dynamo process in three-dimensional helical magnetohydrodynamic turbulence [9], we propose a simple three-

scale model which is able to capture our numerical results. We further show that the Lagrangian dynamics of this condensate can be described by Langevin equations for particles with inertia.

## II. NUMERICAL SIMULATIONS

Let  $\psi$  be the two-dimensional (scalar) stream-function. The velocity and vorticity are  $\mathbf{u} = (\partial_y \psi, -\partial_x \psi)$  and  $\omega = -\nabla^2 \psi$ , respectively. We solve the two-dimensional incompressible Navier–Stokes equations in the vorticity–stream-function formulation, i.e.,

$$\partial_t \omega - J(\psi, \omega) = \nu \nabla^2 \omega + g, \quad (1)$$

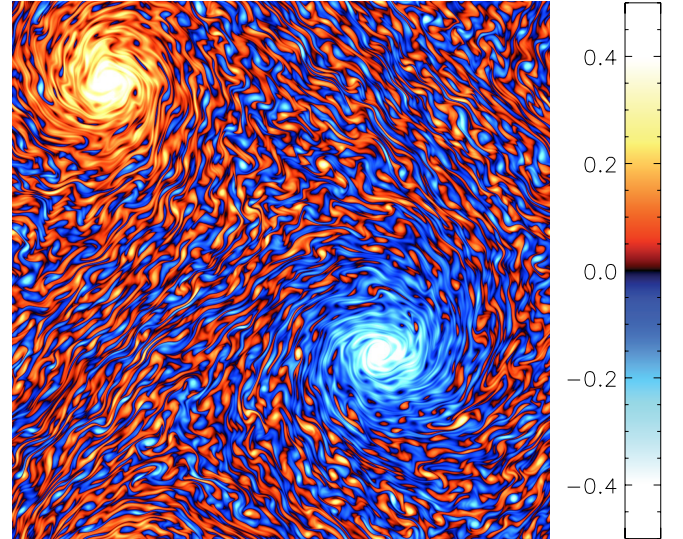


FIG. 1. Color contour of a typical pair of condensate vortices. Red and blue represent positive and negative vorticity in physical space, respectively. The color scale is shown in the color bar on the right, which is chosen to make the fluctuation outside the condensate vortices visible. The vorticity is normalized so that  $\max |\omega| = 1$ .

\* ckch@nordita.org

† dhrua.mitra@gmail.com

‡ brandenb@nordita.org

Name	Inputs			Predictions			Results			Notes
	$\nu$	$k_i$	$k_d$	$\tau_{\overline{E}}$	$E_\infty$	Resolution	$\tilde{\tau}_{\overline{E}}$	$\tilde{E}_\infty$	$\tilde{E}_\infty/E_\infty$	
<b>a16</b>	$10^{-3}$	16	80	500	405	$512^2$	483	323	0.80	
<b>a24</b>	$10^{-3}$	24	91	500	356	$512^2$	520	281	0.79	
<b>a32</b>	$10^{-3}$	32	100	500	308	$512^2$	582	234	0.76	
<b>b16<sup>f</sup></b>	$5 \times 10^{-4}$	16	113	1000	891	$512^2$	—	—	—	single-precision, crashed
<b>b16</b>	$5 \times 10^{-4}$	16	113	1000	891	$512^2$	922	696	0.78	
<b>b24</b>	$5 \times 10^{-4}$	24	129	1000	832	$512^2$	947	643	0.77	
<b>b32</b>	$5 \times 10^{-4}$	32	142	1000	772	$512^2$	970	580	0.75	
<b>c16</b>	$2 \times 10^{-4}$	16	178	2500	2373	$1024^2$	2223	1818	0.76	
<b>c32</b>	$2 \times 10^{-4}$	32	224	2500	2226	$1024^2$	2287	1714	0.77	
<b>c64</b>	$2 \times 10^{-4}$	64	283	2500	1928	$1024^2$	2409	1385	0.72	
<b>c64<sup>b</sup></b>	$2 \times 10^{-4}$	64	283	2500	1928	$512^2$	1985	791	0.41	converge to wrong answer
<b>d16</b>	$10^{-4}$	16	252	5000	4859	$1024^2$	4145	3581	0.74	
<b>d32</b>	$10^{-4}$	32	317	5000	4691	$1024^2$	4006	3349	0.72	
<b>path<sup>i</sup></b>	$5 \times 10^{-4}$	32	142	1000	308	$512^2$	—	580	0.75	restart from saturated <b>b32</b>

TABLE I. List of simulations: the first thirteen simulations are used to verify our three-scale model (16). The last row describes sixteen restart-runs which are initially in saturated states. They are used to verify the properties of  $\Delta r^2$ . The details of the simulations are described in section II.

where the Jacobian determinant is given by

$$J(\psi, \omega) = (\partial_x \psi)(\partial_y \omega) - (\partial_x \omega)(\partial_y \psi). \quad (2)$$

We use periodic boundary conditions with  $L = 2\pi$  and denote the Fourier transform of  $\omega$  by  $\omega_{\mathbf{k}}$ . In equation (1),  $g$  is the vertical component of the curl of an external force at a wavenumber  $\mathbf{k}_i$ . Both  $\mathbf{k}_i$  and  $g$  are taken to be random and white-in-time with zero means and variances

$$\langle \mathbf{k}_i(s) \cdot \mathbf{k}_i(t) \rangle = k_i^2 \delta(t - s), \quad (3)$$

$$\langle g_{\mathbf{k}_i}^*(s) \cdot g_{\mathbf{k}_i}(t) \rangle = f_i^2 k_i^2 \delta(t - s), \quad (4)$$

where  $\langle \cdot \rangle$  denotes ensemble averages. At each time step, we implement the first condition by choosing a random phase. The second condition is achieved by randomly selecting a wavenumber  $\mathbf{k}_i$  in a shell with radius  $k_i$  and then round it off to the nearest grid point in the Fourier space. For this force, the average rate of energy and enstrophy inputs are respectively  $f_i^2$  and  $f_i^2 k_i^2$ .

We use spectral Galerkin schemes in space and a low-storage third-order Runge-Kutta/Crank-Nicolson time stepping scheme [10]. The time steps  $\Delta t$  are chosen with a CFL number of 0.5. The non-linear term is treated explicitly and the diffusion term is treated implicitly. The stochastic forcing is integrated by the Euler-Maruyama method [11]. We use  $N \times N$  grid points with the Galerkin cutoff at  $k_G \equiv \lfloor (N-1)/3 \rfloor + 0.99$ . The value 0.99 is chosen such that the comparison  $k^2 \leq k_G^2$  is accurate enough even in single-precision with  $N \sim 2048$ , although almost all simulations in this paper are done with double-precision.

Our code is implemented in **CUDA C** and runs on graphics processing units (GPUs), which are massively parallel “stream” processors. When using an **nVidia Tesla**

**C2050** graphic card, our code is over an order of magnitude faster than codes running on a single CPU core. On the other hand, because of communication overhead, our code outperforms shared-memory parallel codes running on 32 cores. This speed up allows us to integrate the problem in very long code time and study the saturation of the condensate vortices. We have released our code as an open-source project under the GNU General Public License version 3 (GPLv3). The project is hosted by the Google Code at <http://code.google.com/p/sg2>.

### III. RESULTS

We have performed a series of simulations, **a16** – **d32**, as shown in Table I with different sets of input parameters  $\nu$  and  $k_i$ . In all our simulations, the initial conditions are  $\omega_{\mathbf{k}}(t=0) = 0$ . The domain size  $L = 2\pi$  gives  $k_1 = 1$ . For the forcing amplitude and wavenumber, we choose  $f_i = 1$  and  $k_1 \ll k_i \ll k_d$ , where  $k_d$  is the dissipation wavenumber. We use  $k_d \equiv \eta^{1/6} \nu^{-1/2}$  where  $\eta$  is the rate of enstrophy dissipation. Further details of the runs are given in Table I.

In our simulations, energy inverse cascades to small Fourier modes till  $k_1$  and at this mode forms a condensate. In fig. 2 we plot the total energy,  $E(t) = \sum |u_{\mathbf{k}}(t)|^2/2$  as a function of time for several runs in Table I. For intermediate time, the growth of energy of this condensate is consistent with earlier results [6]. In all the cases for large time  $E$  becomes independent of time. However, this saturation happens at very large times. Essentially this time scale is determined by the viscous time at  $k_1$ , i.e.,  $\tau_\nu = 1/\nu k_1^2$ . This requires very long integration times and hence has not been explored

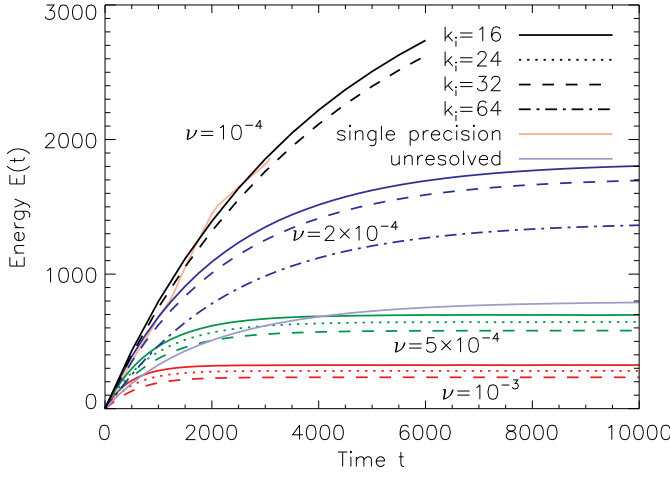


FIG. 2. Un-normalized energy evolution in simulations **a16** – **d32**. The thick red, green, blue, and black curves are for different viscosity  $\nu$  (see labels); while solid, dashed, and dotted styles denote different forcing wavenumber  $k_i$  (see legend). The light red and light blue curve are simulations **b16<sup>f</sup>** and **c64<sup>b</sup>**, respectively. They correspond to single precision and under-resolved simulations respectively.

by earlier simulations. We are able to reach such late times by virtue of using a GPU code.

At later times, most of the total energy comes from the energy of the condensate. Further understanding of the growth and saturation of the condensate can be obtained by studying the shell-integrated energy spectrum  $E_k$ , plotted in fig. 3. Here we have binned the spectrum such that the  $|\mathbf{k}| = k_1, \sqrt{2}k_1, 2k_1$ , and  $\sqrt{5}k_1$  modes have their own data points. The peak of the energy is at the scale of the condensate, there is a valley and a second peak right next to it. The existence of these features is consistent with the plot of the vorticity in real space shown in fig. 1. The vortex pair in real space is described not only by Fourier mode  $k_1$  but also by additional higher harmonics. The symmetry of the vortex pair determines the Fourier amplitudes of the higher harmonics in the Fourier space, which is shown in the inset of fig. 3. The most energetic  $k_1$  modes are marked with black circles. Their “first harmonics” with radius  $\sqrt{5}k_1$  are in dark gray. Other available modes with even  $k_x + k_y$  are marked as open circles. These open circles form exactly the valley in the spectrum. The spectrum has three prominent ranges, the condensate, the inverse cascade and the forward cascade. This motivates us to make a three scale model to describe the time evolution of the energy of the condensate.

### A. Energy and enstrophy evolution

Starting with the shell-integrated energy spectrum,  $E_k$ , the total energy, enstrophy, and palinstrophy can be computed by  $E = \int E_k dk$ ,  $Z = \int k^2 E_k dk$ , and

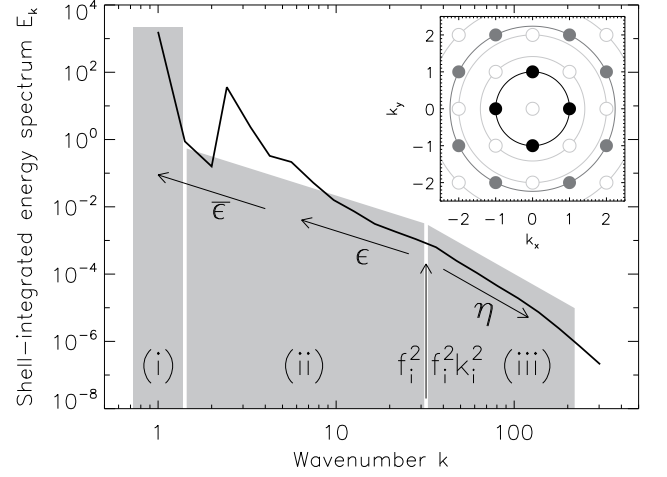


FIG. 3. Energy spectrum in simulation **c32**. The thick solid line is the energy spectrum  $E_k$  computed at  $t = 10000$ . The valley right next to the condensate mode is physical. It corresponds to the  $|\mathbf{k}| = \sqrt{2}k_1$  and  $2k_1$  modes, which have even  $k_x + k_y$  (see inset). The gray areas show our three-scale model, which contains a large amount of energy at  $k_1$  [zone (i)] and a broken power law in other wavenumbers [zone (ii) and (iii)].

$P = \int k^4 E_k dk$ , respectively. Together with the average energy and enstrophy input, the evolution of these quantities is governed by the following equations

$$\partial_t E = -2\nu Z + f_i^2, \quad (5)$$

$$\partial_t Z = -2\nu P + f_i^2 k_i^2. \quad (6)$$

Our three scale model is constructed in the following fashion. We refer to the corresponding wavenumber ranges as zones (i) through (iii). (i) At the wavenumber of the box  $k_1$ , we have the condensate modes, which contain most of the energy at saturation. We use the shorthand  $\bar{E}(t)$  to denote the time-dependent energy at this Fourier mode. (ii) In the range  $k_1 < k \leq k_i$ , the energy inverse cascades from the forcing wavenumber  $k_i$  and forms an  $E_k \sim k^{-5/3}$  spectrum. Note that the enstrophy spectrum  $Z_k = k^2 E_k$  peaks at the forcing wavenumber  $k_i$ . (iii) The forward enstrophy cascade in the small scales gives the spectrum  $E_k \sim k^{-3}$  with a sharp cutoff at  $k = k_d$ . It is necessary to assume this cutoff to prevent the ultraviolet divergence of the total enstrophy and palinstrophy, although not total energy.

Let us now denote by  $\bar{E}$  the energy in the  $k = k_1$  mode, i.e., the condensate, and by  $E'$  the energy of the rest of the system, i.e.,  $E = \bar{E} + E'$ . We often call them the mean and the fluctuating part respectively. Similar notation is applied to enstrophy and palinstrophy too. We can then split the energy equation (5) into two parts, namely,

$$\partial_t \bar{E} = -2\nu k_1^2 \bar{E} + \bar{\epsilon}, \quad (7)$$

$$\partial_t E' = -2\nu Z' + f_i^2 - \bar{\epsilon}, \quad (8)$$

where  $\bar{\epsilon}$  is the inverse energy transfer rate to the condensate. Similarly, with the help of (7), we can rewrite

equation (6) as

$$\partial_t Z' = -2\nu P' + f_i^2 k_i^2 - k_1^2 \bar{\epsilon}. \quad (9)$$

The last term  $k_1^2 \bar{\epsilon}$  describes the enstrophy transfer rate to the condensate. Its existence implies that, although most of the enstrophy is transferred toward smaller scales, there is a small *leakage* towards the largest scale.

Equations (7)–(9) are exact but not closed. Hence, it is not yet possible to solve them simultaneously. We parameterize the fluctuating palinstrophy and enstrophy by  $\gamma$  and  $\Gamma$  such that

$$P' \equiv P - k_1^4 \bar{E} = \gamma k_d^2 Z', \quad (10)$$

$$Z' \equiv Z - k_1^2 \bar{E} = \Gamma k_i^2 E'. \quad (11)$$

Substituting the above equations into (8) and (9) we obtain two simultaneous equations. We then eliminate  $\bar{\epsilon}$  between them to obtain a dynamical equation for  $Z'$ , which can be solved to obtain

$$Z'(t) = Z'_\infty \left[ 1 - e^{-(t-t_0)/\tau_{Z'}} \right]. \quad (12)$$

where we have used the initial condition  $Z'(t_0) = 0$  and

$$Z'_\infty \equiv \frac{f_i^2}{2\nu} \frac{k_i^2 - k_1^2}{\gamma k_d^2 - k_1^2}, \quad (13)$$

with characteristic time scale

$$\tau_{Z'} \equiv \frac{1}{2\nu\Gamma k_i^2} \frac{\Gamma k_i^2 - k_1^2}{\gamma k_d^2 - k_1^2}. \quad (14)$$

Now note that  $\tau_{Z'} \approx 1/2\nu\gamma k_d^2$  is substantially faster than the time scale of saturation of  $\bar{E}$ , which is of the order of  $\nu k_1^2$ . Hence, in equation (7) we can replace  $\bar{\epsilon}$  by its value at large time,  $\bar{\epsilon}_\infty$ , which can be obtained by replacing  $Z'$  by  $Z'_\infty$  in equation (8),

$$\bar{\epsilon}_\infty \equiv \lim_{t \rightarrow \infty} \bar{\epsilon}(t) = f_i^2 - 2\nu Z'_\infty = f_i^2 \frac{\gamma k_d^2 - k_i^2}{\gamma k_d^2 - k_1^2}. \quad (15)$$

Substituting this back in (7) and solving for  $\bar{E}$  we obtain,

$$\bar{E}(t) = \bar{E}_\infty \left[ 1 - e^{-(t-t_0)/\tau_{\bar{E}}} \right]. \quad (16)$$

where we have used the initial condition  $\bar{E}(t_0) = 0$ . This solution saturates to

$$\bar{E}_\infty \equiv \frac{f_i^2}{2\nu k_1^2} \frac{\gamma k_d^2 - k_i^2}{\gamma k_d^2 - k_1^2} \quad (17)$$

with a characteristic time scales

$$\tau_{\bar{E}} \equiv 1/2\nu k_1^2. \quad (18)$$

To obtain  $\bar{E}_\infty$  we need to estimate  $k_d$  and  $\gamma$ . For the former we use the dimensional estimate,

$$k_d = f_i^{1/3} (k_i^2 - k_1^2)^{1/6} \nu^{-1/2} \quad (19)$$

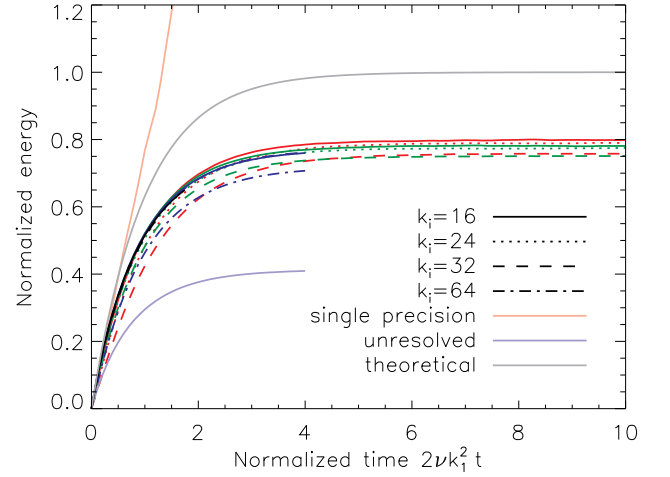


FIG. 4. Energy evolution in simulations **a16** – **d32**. The thick red, green, blue, and black curves are for different viscosity  $\nu$  (see labels in fig. 2); while solid, dashed, and dotted styles denote different forcing wavenumber  $k_i$  (see legend). We normalize the energy and time using the results from our three-scale model. Almost all the curves collapse onto each other. The light gray, light red, and light blue curve are the theoretical prediction, **b16<sup>f</sup>**, and **c64<sup>b</sup>**, respectively.

To estimate the latter we assume that in the inverse cascade,  $E_k \sim k^{-5/3}$  and in the direct cascade  $E_k \sim k^{-3}$ . These two power laws must match at  $k = k_i$ . Using these the dimensionless number  $\gamma$  can be estimated to be

$$\gamma \approx \frac{2}{3 + 4 \ln(k_d/k_i)} \lesssim 1. \quad (20)$$

The model no longer has any free parameter. In fig. 4, we now plot the energy as a function of time with the vertical axis normalized by  $\bar{E}_\infty$  and also scale the time axis by  $\tau_{\bar{E}}$ . This collapses all the different time traces providing support to our three scale model. Note that the nontrivial expression of  $\bar{E}_\infty$  given in (17) is necessary to obtain this collapse. Note also that the expressions for  $\bar{E}_\infty$  and  $Z'_\infty$  can be derived directly demanding that at late time we reach a stationary state, with  $\partial_t E = \partial_t Z = 0$ . Imposing this condition to (5) and (6), equations (17) and (13) follow.

Although all the results from different simulations collapse on each other this collapsed curve lies systematically below the analytical solution shown as light gray curve in fig. 4. To estimate this discrepancy we fit the numerical curves by (16) to find numerical values for  $E_\infty$  and  $\tau_{\bar{E}}$ . These values are compared with their theoretical prediction in Table I. The timescales agree to a good accuracy. The ratios between the theoretical  $E_\infty$  and the fitted  $\bar{E}_\infty$  and are listed in the tenth column of Table I. The average of these ratios (not including **b16<sup>f</sup>**, **c64<sup>b</sup>**, and **path<sup>i</sup>**) is  $\zeta \equiv \langle \bar{E}_\infty / E_\infty \rangle \approx 0.76$ . We speculate that this systematic difference exists because we have ignored the second (smaller) peak in the spectrum in our three scale model.

Comments on the remaining run in Table I are now in order. The light blue curve is for the **c64<sup>b</sup>** run. Although the curve looks perfectly reasonable, the resolution of the simulation,  $512^2$ , which gives  $k_G \approx 170$ , is too low to resolve the actual enstrophy dissipation wavenumber  $k_d = 283$ . Because spectral Galerkin methods have very little numerical dissipation, the forward cascaded enstrophy cannot be removed, which artificially increases  $Z'_\infty$  and decrease  $\bar{\epsilon}_\infty$ . Hence, the steady state energy  $E_\infty$  converges to an (incorrect) lower value. In the language of numerical analysis, this is an inconsistent numerical solution.

The light red curve in fig. 4 is the **b16<sup>f</sup>** run, which uses single-precision floating-point numbers to represent  $\omega_k$  instead of double-precision. The numerical solution behaves properly at the beginning but starts to diverge from the true solution around  $t = 1000 = \tau_E$ . This is not surprising because the relative round off error of single-precision numbers is about  $\sim 10^{-7}$ . A random walk of round off error in  $\omega_k$  leads to a linear grow of error in the energy. Indeed, there are roughly  $10^7$  steps by the time  $t = \tau_E$ , which gives the order of unit error seen in the figure. To date a significant fraction of scientific computing in GPUs are done with single precision. This turns out not to be sufficient for our purpose.

## B. Movement of Condensate Vortices

After studying the saturation level and time scale, we focus on the movement of the condensate vortices at late times. The last row in Table I represents sixteen different simulations **path<sup>85</sup>** – **path<sup>100</sup>**. The superscripts in the names have the following meaning. For **path<sup>i</sup>**, we pick the  $i$ -th output file of **b32** and restart the simulation each time with a different realization of the random force. In other words for the  $i$ -th run the random number generators are started with seed  $i$ . We then evolve the solutions for another  $t = 10\tau_E$ . Because **b32** has reached saturated state long before the 85-th output, the energy levels remain almost constant in all these simulations. The results are sixteen ensemble of the saturated solutions. A movie of one of these runs shows that the condensate wanders around randomly inside the domain.

The positions of the condensate vortices are simply given by the phases of the  $k_1$  modes. We unfold the trajectories from the computational domain  $[0, 2\pi)^2$  into  $\mathbb{R}^2$  and shift their starting points to the origin. We label the  $x$ - and  $y$ -displacements by  $\Delta x$  and  $\Delta y$ , respectively and plot such a trajectory (for **path<sup>100</sup>**) in figure 5. The small gray box near the origin shows the size of the original domain  $[0, 2\pi)^2$ . With the unfolded trajectories, we compute the displacement square  $\Delta r^2 = \Delta x^2 + \Delta y^2$  for all sixteen **path<sup>i</sup>** runs. For each simulation, we plot a gray curve in fig. 6. The thick solid curve shows their (ensemble) average. Below we describe a way to model the motion of this condensate.

As before we define a “mean” vorticity by

$$\bar{\omega}(\mathbf{x}) \equiv \sum_{|\mathbf{k}|=k_1} \omega_{\mathbf{k}} e^{i\mathbf{k}\cdot\mathbf{x}} \quad (21)$$

Averaging the Navier–Stokes equation we obtain,

$$\partial_t \bar{\omega} + \nabla \cdot (\bar{\mathbf{u}} \bar{\omega}) = -\nabla \cdot \bar{\mathcal{F}} + \nu \nabla^2 \bar{\omega}. \quad (22)$$

In the above equation,  $\bar{\mathcal{F}} \equiv \overline{\mathbf{u} \omega} - \bar{\mathbf{u}} \bar{\omega}$  is the space-dependent mean vorticity flux. Note that the forcing  $g$  is at small wavenumber  $k_i \gg k_1$  so its mean vanishes. It is straightforward to show that the non-linear term  $\nabla \cdot (\bar{\mathbf{u}} \bar{\omega})$  vanishes identically. Both the creation and the movement of the condensate, therefore, must be due to the flux  $\bar{\mathcal{F}}$ .

We now model this mean vorticity flux using usual technique of mean-field dynamo theory [12, 13]

$$\bar{\mathcal{F}}_i = \alpha_i \bar{\omega} + \beta_{ij} \partial_j \bar{\omega}. \quad (23)$$

The transport coefficients  $\alpha_i$  and  $\beta_{ij}$  are constants in space because we consider only the  $k_1$  modes. The mean-field equation then becomes

$$(\partial_t + \alpha_i \partial_i) \bar{\omega} = (\nu \delta_{ij} - \beta_{ij}) \partial_i \partial_j \bar{\omega}. \quad (24)$$

The coefficient  $\alpha_i$  cannot change the amplitude of the condensate. It can be thought of as the *Lagrangian velocity* of the condensate vortex. The inverse energy cascade, therefore, must be described by the *anti-diffusion*.

Expanding  $\nabla \cdot \bar{\mathcal{F}}$ , there are only two independent Fourier coefficients,  $\bar{\mathcal{F}}_{x,k_1\hat{\mathbf{x}}}$  and  $\bar{\mathcal{F}}_{y,k_1\hat{\mathbf{y}}}$ , that enter the mean field equation (the first subscript denotes component, the second one denotes wavevector). Comparing with our parameterization (23), it is clear that

$$\alpha_x = \text{Re} \frac{\bar{\mathcal{F}}_{x,k_1\hat{\mathbf{x}}}}{\omega_{k_1\hat{\mathbf{x}}}}, \quad \alpha_y = \text{Re} \frac{\bar{\mathcal{F}}_{y,k_1\hat{\mathbf{y}}}}{\omega_{k_1\hat{\mathbf{y}}}}; \quad (25)$$

$$\beta_{xx} = \text{Im} \frac{\bar{\mathcal{F}}_{x,k_1\hat{\mathbf{x}}}}{k_1 \omega_{k_1\hat{\mathbf{x}}}}, \quad \beta_{yy} = \text{Im} \frac{\bar{\mathcal{F}}_{y,k_1\hat{\mathbf{y}}}}{k_1 \omega_{k_1\hat{\mathbf{y}}}}. \quad (26)$$

It is clear that  $\langle \beta_{xx} \rangle = \langle \beta_{yy} \rangle = \nu$  at saturation.

The value of  $\alpha$ , however, is much more difficult to obtain because there is no constraint by conservation laws. We can only perform a rough estimate: the flux  $\bar{\mathcal{F}}$  is a convolution in Fourier space. Given that  $k_1^2 \bar{E}_\infty / Z'_\infty \gg 1$ , the condensate-fluctuation interaction dominates,

$$\bar{\mathcal{F}} \sim \mathbf{u}_{\sqrt{2}k_1} \bar{\omega}, \quad (27)$$

where  $\mathbf{u}_{\sqrt{2}k_1}$  represents the typical value of a band-pass filtered velocity. Comparing the estimate with equation (25) and employing the results from our three-scale model, we obtain

$$\langle \alpha^2 \rangle \sim k_1 E_{\sqrt{2}k_1} \approx \frac{f_1^2}{2\nu k_d^2} \left( \frac{k_1}{k_1} \right)^{2/3} = \frac{f_1^{4/3}}{2k_1^{2/3}}. \quad (28)$$



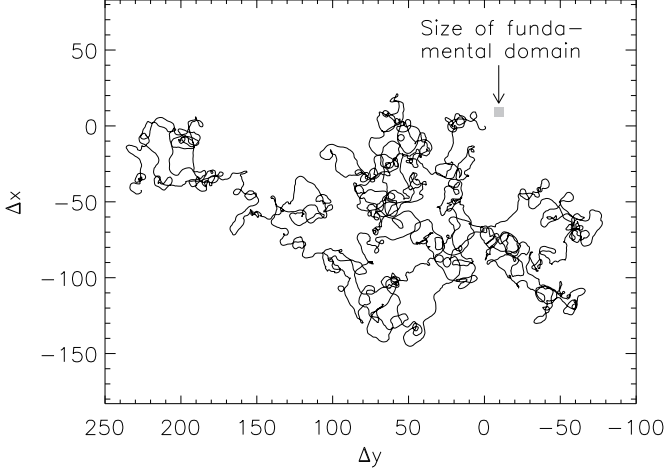


FIG. 5. Unfolded trajectory of a condensate vortex in simulation  $\text{path}^{100}$ . The computational domain is  $[0, 2\pi)^2$  (shown as a gray box near the origin). We first unfold the trajectory into  $\mathbb{R}^2$  and then shift the initial position to the origin.

Note that the same argument leads to  $\langle \beta^2 \rangle \sim k_1^{-2} \langle \alpha^2 \rangle$ . Fortunately, it does not contradict  $\langle \beta \rangle = \nu$ .

Let us now take  $\alpha$  to be statistically independent of  $\bar{\omega}$ . Equation (24) then becomes the equation of a passive scalar advected by a random velocity  $\alpha$ . As  $\alpha$  has a stationary variance (28) its simplest model would be an Ornstein-Uhlenbeck process [14–16]

$$\partial_t \alpha = -\alpha/\tau_\alpha + \phi, \quad (29)$$

In the above phenomenological equation,  $1/\tau_\alpha$  is an effective drag coefficient and  $\phi$  is an effective stochastic forcing. Because  $\alpha$  is at a scale close to the condensate, we model the effective forcing  $\phi$  by Gaussian white noise with zero mean and variance equal to  $\xi \bar{\epsilon}$ . Here  $\bar{\epsilon}$  is the mean energy input to the condensate and  $\xi$  is a tunable parameter. Standard Itô calculus gives

$$\langle \alpha(t) \rangle = \alpha(0) e^{-t/\tau_\alpha}, \quad (30)$$

$$\begin{aligned} \langle \alpha(s) \cdot \alpha(t) \rangle &= \alpha(0)^2 e^{-(t+s)/\tau_\alpha} \\ &+ \xi f_i^2 \frac{\gamma k_d^2 - k_i^2}{\gamma k_d^2 - k_i^2} \tau_\alpha \left[ e^{-(t-s)/\tau_\alpha} - e^{-(t+s)/\tau_\alpha} \right], \end{aligned} \quad (31)$$

where the second equation is only valid for  $s < t$ .

By requiring  $\langle \alpha(t)^2 \rangle = \langle \alpha^2 \rangle$  for arbitrary large  $t$ , we can solve for the time scale

$$\tau_\alpha = \frac{1}{2\xi f_i^{2/3} k_1^{2/3}} \frac{\gamma k_d^2 - k_i^2}{\gamma k_d^2 - k_i^2}. \quad (32)$$

Furthermore, starting with an expected initial condition  $\alpha(0)^2 = \langle \alpha^2 \rangle$  allows us to simplify the correlation to

$$\langle \alpha(s) \cdot \alpha(t) \rangle = \langle \alpha^2 \rangle e^{-(t-s)/\tau_\alpha}. \quad (33)$$

The displacement of the condensate can now be solved by using the simple equation  $\partial_t \mathbf{r} = \alpha$ . Let  $\Delta \mathbf{r}(t) \equiv$

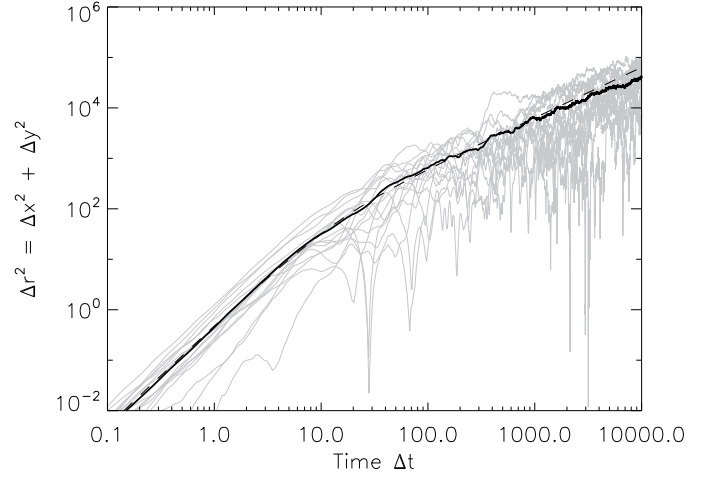


FIG. 6. The gray curves are the displacement square  $\Delta r^2$  for all sixteen  $\text{path}^1$  runs. The thick solid curve shows their average. The dashed line, which is indistinguishable from the solid line, is the solution (34) with parameter  $\xi = 0.1$ .

$\mathbf{r}(t) - \mathbf{r}(0)$  be the displacement from the initial position, we have

$$\begin{aligned} \langle \Delta r(t)^2 \rangle &= 2 \int_0^t dt' \int_0^{t'} ds' \langle \alpha(s') \cdot \alpha(t') \rangle \\ &= 2 \langle \alpha^2 \rangle \tau_\alpha \left[ t + \tau_\alpha (e^{-t/\tau_\alpha} - 1) \right]. \end{aligned} \quad (34)$$

The same equation also describes Brownian motion of a inertial particle. Its asymptotic behavior is

$$\langle \Delta r(t)^2 \rangle \approx \begin{cases} \langle \alpha^2 \rangle t^2, & t < \tau_\alpha; \\ 2 \langle \alpha^2 \rangle \tau_\alpha t, & t > \tau_\alpha. \end{cases} \quad (35)$$

The early time behavior is completely determined by  $\langle \alpha^2 \rangle$ ; while the free parameter  $\xi$  controls only the Brownian motion of the condensate vortex at late time.

Now we compare our model with results from simulations. The dashed curve in fig. 6 is equation (34) with a parameter  $\xi = 0.1$ , which corresponds to  $\tau_\alpha = 6.384$ . It is practically indistinguishable from the thick line except at later times. Note that at small times (which are still larger than  $\tau_E$ ) the condensate movement is independent of  $\xi$ . Hence the agreement between the thick solid and dashed curves for  $\Delta t < \tau_\alpha$  provides support to our phenomenological model. Although we are not able to derive  $\xi$ , the late time agreement suggests that the condensate motion is Brownian for  $\Delta t > \tau_\alpha$ .

#### IV. DISCUSSIONS

In this paper, we use a three-scale model to derive the saturate time scales and saturation levels of the condensate and turbulent fluctuation in 2D hydrodynamic turbulence. This requires integrating the two dimensional

Navier–Stokes equations for very long time. This has been made possible by virtue of the high performance of the GPUs. We use the Ornstein-Uhlenbeck process as a phenomenological model to describe the movement of condensate vortex. In terms of the saturation time scales  $\tau_{\overline{E}}$  and  $\tau_{Z'}$ , the DNS agree quite well with the analytical predictions. The saturation levels are, however, off by a constant factor  $\zeta = 0.76$ . We speculate that this disagreement is because our three-scale model ignores the second peak in the energy spectrum. We have checked that it is not possible to remedy this problem by just changing  $k_1$  in our model to an effective wavenumber  $k_{\text{cond}} \gtrsim k_1$ . A more sophisticated model is needed.

The spectral valley right next to the condensate in fig. 3, to the authors’ knowledge, is not seen in previous numerical studies such as [8, 17], possibly because these earlier studies have not reached the late saturated stage we study. The spectrum obtained from atmospheric data [18] or from direct numerical simulations with Ekman friction [19] would also not have these features as in those cases energy from the large scales are removed by friction.

Before we conclude, we should point out that the direct (forward) enstrophy flux

$$\eta_{\text{dir}} \equiv \eta_{\infty} \approx f_i^2(k_i^2 - k_1^2) \quad (36)$$

is smaller than the enstrophy input  $f_i^2 k_i^2$  in our three-scale model. There is no inconsistency here. Their difference is simply the (very small) inverse enstrophy *leakage*

$$\eta_{\text{inv}} \equiv f_i^2 k_i^2 - \eta_{\text{dir}} \approx f_i^2 k_1^2 \quad (37)$$

that we commented on for equation (9). The property  $\eta_{\text{inv}} \ll \eta_{\text{dir}}$  is nothing magical. It is a consequence of the broken power law in our three-scale model.

Similarly, we can check how the direct (forward) energy *leakage*  $\epsilon_{\text{dir}}$  compare with the inverse cascade  $\epsilon_{\text{inv}}$ . Recalling that  $\bar{\epsilon}$  is only the inverse energy transfer rate at  $k_1$ , we need to add the contribution from  $2\nu Z'$ ,

$$\epsilon_{\text{inv}} \equiv \bar{\epsilon} + 3\nu\gamma Z'_{\infty} \approx f_i^2 \left[ 1 - \left( 1 - \frac{3}{2}\gamma \right) \frac{k_i^2}{\gamma k_d^2} \right], \quad (38)$$

$$\epsilon_{\text{dir}} \equiv 4\nu\gamma \ln \frac{k_d}{k_i} Z'_{\infty} \approx f_i^2 \left( 1 - \frac{3}{2}\gamma \right) \frac{k_i^2}{\gamma k_d^2}. \quad (39)$$

Using the original definition (20), it is easy to verify that  $1 - 3\gamma/2 \lesssim 1$ , which allows us to conclude  $\epsilon_{\text{inv}} \gg \epsilon_{\text{dir}}$ . Most of the input energy is inversely cascaded and dissipated at the condensate. Note that the above approximations are made at the same order. The fact that  $\epsilon_{\text{inv}} + \epsilon_{\text{dir}} = f_i^2$  holds, therefore, shows the consistence of our model.

Note finally that our work stresses the fact that as in three dimensional turbulence [20], the order of taking the limit of long time ( $t \rightarrow \infty$ ) and small viscosity ( $\nu \rightarrow 0$ ) is crucial in two dimensional turbulence too. Specifically, taking the limit  $\nu \rightarrow 0$  first leads to a (linear) divergence in time

$$\lim_{t \rightarrow \infty} \left( \lim_{\nu \rightarrow 0} \overline{E} \right) = \lim_{t \rightarrow \infty} f_i^2 t. \quad (40)$$

We must take the limits in the correct order, which is,

$$\begin{aligned} \lim_{\nu \rightarrow 0} \left( \lim_{t \rightarrow \infty} \overline{E} \right) &= \lim_{\nu \rightarrow 0} \left( \frac{f_i^2}{2\nu k_1^2} \frac{\gamma k_d^2 - k_i^2}{\gamma k_d^2 - k_1^2} \right) \\ &= \lim_{\nu \rightarrow 0} \frac{f_i^2}{2\nu k_1^2}. \end{aligned} \quad (41)$$

The system can then reach a steady state as long as the viscosity remains non-zero, even without the Ekman term.

## ACKNOWLEDGMENTS

All simulations presented in this paper were done on the **Zorn** cluster in PDC and the **Platon** cluster in Lunarc. CKC is supported by a Nordita fellowship. CKC and AB thank John Bowman and Malcolm Roberts for insightful discussions, which motivated this work. All three authors thank the organizers of the *Nature of Turbulence* workshop and are grateful to the hospitality by UCSB and KITP. Financial support from European Research Council under the AstroDyn Research Project 227952 is gratefully acknowledged.

- 
- [1] R. H. Kraichnan, *Physics of Fluids* **10**, 1417 (1967).
  - [2] C. E. Leith, *Physics of Fluids* **11**, 671 (1968).
  - [3] G. K. Batchelor, *Physics of Fluids* **12**, 233 (1969).
  - [4] L. M. Smith and V. Yakhot, *Physical Review Letters* **71**, 352 (1993).
  - [5] L. M. Smith and V. Yakhot, *Journal of Fluid Mechanics* **274**, 115 (1994).
  - [6] M. Chertkov, C. Connaughton, I. Kolokolov, and V. Lebedev, *Physical Review Letters* **99**, 084501 (2007), arXiv:nlin/0612052.
  - [7] H. Xia, H. Punzmann, G. Falkovich, and M. G. Shats, *Physical Review Letters* **101**, 194504 (2008), arXiv:0806.3116 [physics.flu-dyn].
  - [8] C. V. Tran and J. C. Bowman, *Phys. Rev. E* **69**, 036303 (2004).
  - [9] A. Brandenburg, *Astrophys. J.* **550**, 824 (2001), arXiv:astro-ph/0006186.
  - [10] J. H. Williamson, *Journal of Computational Physics* **35**, 48 (1980).
  - [11] D. J. Higham, *SIAM Review* **43**, 525 (2001).

- [12] A. Brandenburg and B. V. Rekowski, A&A **379**, 1153 (2001), arXiv:astro-ph/0106280.
- [13] A. Brandenburg and K. Subramanian, Physics Reports **417**, 1 (2005), arXiv:astro-ph/0405052.
- [14] G. E. Uhlenbeck and L. S. Ornstein, Physical Review **36**, 823 (1930).
- [15] S. Chandrasekhar, Reviews of Modern Physics **15**, 1 (1943).
- [16] M. C. Wang and G. E. Uhlenbeck, Reviews of Modern Physics **17**, 323 (1945).
- [17] V. Borue, Physical Review Letters **72**, 1475 (1994).
- [18] K. S. Gage and G. D. Nastrom, Radio Science **20**, 1339 (1985).
- [19] P. Perlekar, S. S. Ray, D. Mitra, and R. Pandit, Physical Review Letters **106**, 054501 (2011), arXiv:1009.1494 [physics.flu-dyn].
- [20] U. Frisch, *Turbulence: The legacy of A. N. Kolmogorov* (Cambridge University Press, 1995).